Available online at www.sciencedirect.com
ScienceDirect
Trans. Nonferrous Met. Soc. China 28(2018) 1103−1113
Transactions of Nonferrous Metals Society of China
www.tnmsc.cn

Effect of limestone ores on grain refinement of as-cast commercial AZ31 magnesium alloys

Xuan LIU[1], Si-qi YIN[2], Zhi-qiang ZHANG[2], Qi-chi LE[2], Ji-lai XUE[1]

1. School of Metallurgical and Ecological Engineering, University of Science and Technology Beijing, Beijing 100083, China;
2. Key Lab of Electromagnetic Processing of Materials, Ministry of Education, Northeastern University, Shenyang 110819, China

Received 3 February 2017; accepted 18 September 2017

Abstract: The grain refinement of the as-cast AZ31 alloys by limestone particles was investigated by grain refining tests and microstructure observations. The results show that the limestone particles have a good grain refining potency, which is deeply related to the addition level of limestone and melting temperature. The optimal addition level and melting temperature are 2.0% (mass fraction) and 720 °C, respectively. The average grain size of AZ31 alloy is reduced from (556±60) to (236±22) μm. The sound grain refining by raw limestone particles has a good anti-fading capacity without any significant grain coarsening in a 40 min holding time. The concerned grain refining mechanism should be attributed to the inoculated Al−C and Al−C/Al−Mn−(Fe) nuclei. Ultrasonic treatment can enhance the grain refining efficiency of limestone particles through cavitation-enhanced nucleation mechanism.

Key words: AZ31 magnesium alloy; grain refinement; limestone ore; microstructure; ultrasonic treatment

1 Introduction

Mg−Al alloys should be the most commercially used, because of their high castabilty and low cost, etc. Significant researches have been conducted to investigate the grain refinement of Mg−Al alloys, such as melt superheating technique, the Elfinal processes, carbon inoculation, deliberate addition of alloying elements and other inoculants [1−4]. Among these researches, carbon inoculation is considered to be the most effective grain refiner for Mg−Al alloys, and have been used for decades. The sound grain refinement by carbon inoculation is mostly supported by the formed Al_4C_3 nuclei [5], which is in good crystallographic match to the magnesium using the edge-to-edge model [6].

There are many carbon sources tried as grain refiners of Mg−Al alloys. JIN et al [7] have investigated the effects of C_2Cl_6 on grain refinement and mechanical properties of AZ31 magnesium alloy. LU et al [8] studied the grain refining efficiency of Al_4C_3 on Mg−Al alloys, while some carbonates were also used to refine AZ31 alloys [9]. Meanwhile, YANO et al [10] even used pure carbon powders to refine Mg−Al alloys and received good grain refinement. Among these sources, the carbonate could be one of the most effective grain refiners on refining the Mg−Al based alloys. KIM et al [11] reported that $MnCO_3$ could well refine the as-cast AZ91 alloy by inoculating heterogeneous nuclei Al_4C_3 and MgO particles as well as the melt agitation due to the release of CO_2 gas. Thus, carbonate might be a potential grain refiner widely used in magnesium industry. However, it is not quite acceptable to add too much carbonate as a state of chemical reagent, due to its considerable price.

Thus, this work aims at finding a cut-price grain refiner which could be widely used for Mg−Al based alloys. Those uneconomic chemical reagents (such as $MgCO_3$ and $CaCO_3$) are replaced with the low-cost raw limestone particles to refine the commercial AZ31 alloys. The grain refining potency and concerned mechanism will also be discussed.

Foundation item: Project (2016YFB0301104) supported by National Key Research and Development Program of China
Corresponding author: Qi-chi LE; Tel: +86-24-83683312; E-mail: qichil@mail.neu.edu.cn
DOI: 10.1016/S1003-6326(18)64746-6

2 Experimental

Figure 1(a) shows the photograph of the raw limestone used in this work. The grey raw limestone is dug from Yingkou, Liaoning Province, China. They own a dense structure with fine grains and some coarse polygonal grains, as shown in Fig. 1(b). Table 1 shows the chemical composition of the raw limestone. It could be seen that the raw limestone mainly consisted of $CaCO_3$ and a small amount of $MgCO_3$, Al_2O_3 and SiO_2. Before addition, the raw limestone was mechanically smashed into small particles, as shown in Fig. 1(c). The limestone particles have a size distribution of 1−5 μm, as shown in Fig. 1(d).

The commercial purity AZ31 ingots (chemical composition: Al 2.92%, Zn 0.61%, Mn 0.42%, Fe ≤0.004% and Mg Bal.) were melted in mild steel crucibles heated by the electrical resistance furnace. The amount of melted AZ31 was 0.8 kg in each trial. A 0.5 L/min cover gas of CO_2+0.5%SF_6 was used to protect the melts from burning and oxidation. The melts were heated to 680, 720 and 760 °C, respectively. The limestone particles were well mixed with flux (46% $MgCl_2$, 40% KCl, 8% $BaCl_2$ and 6% CaF_2) before addition, and the addition levels were 0.1%, 0.3%, 0.5%, 1.0% and 2.0%, respectively. During limestone addition, the melts were stirred for 3 min by hand tool to ensure adequate contact, and the melt temperature fluctuation was controlled to be ±5 °C. The melts were then held at the adding temperature for additional 10 min before casting. The chemical reagent ($CaCO_3$, >99.9%, Kermel^{TM}, <5 μm) were also used for contrast tests. Furthermore, the ultrasound was also involved to investigate the combining grain refining effects of both ultrasound and limestone addition.

Table 1 Main chemical composition of raw limestone (mass fraction, %)

SiO_2	Al_2O_3	Fe_2O_3	CaO	MgO
1.62	1.31	0.57	49.52	2.66

Gravity casting in *d*60 mm permanent mold was applied to preparing samples. On the other hand, suction casting in *d*12 mm quartz tubes as demonstrated in Ref. [12] was also conducted to investigate the effect of holding time on the grain refining potency. Each sample

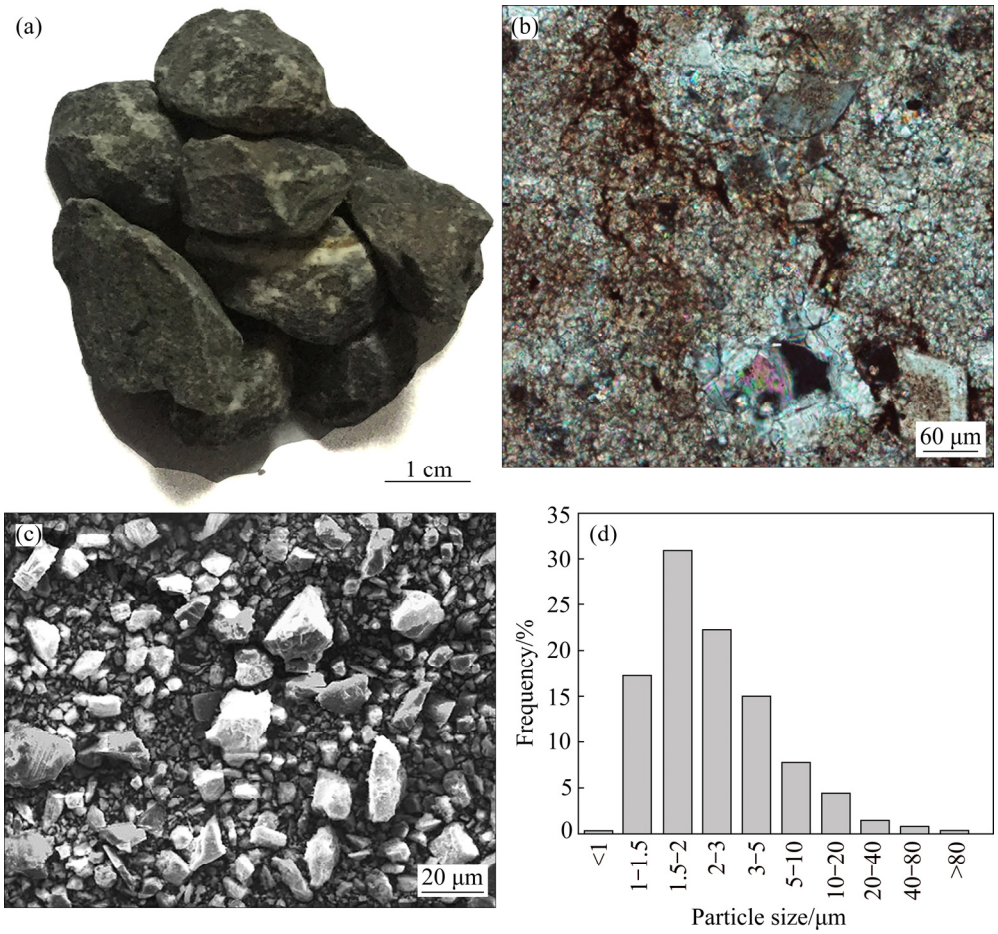

Fig. 1 Raw limestone used in this work: (a) Photograph of limestone; (b) Microscopic graph of limestone (projection under cross-polarized light); (c) SEM image of smashed limestone; (d) Particle size distribution of smashed limestone

was sectioned at the same position (for suction casting, 200 mm from the base; for gravity casting, 20 mm from the base). The samples were polished and etched by a mixed acid solution (3 g picric acid, 2 mL glacial acetic acid, 5 mL alcohol and 50 mL water). The grain structures were examined using optical microscopy. The mean grain size at the center of each sample was measured using the linear intercept method, and five data of measured grain size were averaged. The grain refining efficiency has also been calculated by the equation, as follows:

$$\eta=(d_{\text{untreated}}-d_{\text{inoculated}})/d_{\text{untreated}} \quad (1)$$

where η is the grain refining efficiency; $d_{\text{untreated}}$ and $d_{\text{inoculated}}$ are the measured grain sizes of the untreated and inoculated alloys, respectively.

The microstructures were further examined using scanning electron microscopy with energy dispersive X-ray (EDX) analysis capabilities. The phase analyses were performed with an X-ray diffractometer (XRD), and the scanning angles were 15°−90° with a speed of 8 (°)/min. The XRD patterns were indexed using PDF standard card (2004).

3 Results

3.1 Grain refining potency of limestone

Figure 2 shows the grain refining results of limestone additions on the gravity casting AZ31 alloys at 720 °C. The unmodified AZ31 alloy has coarse grains (Fig. 2(a)) with an average grain size of (556±60) μm. After 0.1% limestone particles are added, the grain size is slightly reduced, as shown in Fig. 2(b). The grain size of modified AZ31 alloy is not significantly reduced until the limestone addition is over 0.5%. The macrostructure with 0.5% limestone addition is fine and uniform, as shown in Fig. 2(d). When the limestone addition reaches 2%, the grain size is almost cut by half to (236±22) μm, as shown in Fig. 2(f). The grain refining efficiency is as high as 58%.

Figure 3 shows the grain refining results of limestone addition at other inoculating temperatures. The grain size of AZ31 alloys still reduces with the increasing limestone addition. Meanwhile, it also reduces as the inoculating temperature increases from 680 to 760 °C. However, the initial grain size cast at 760 °C is much finer than that at 680 °C. Figure 4(a) shows the average grain size of AZ31 alloy versus addition level of limestone at the investigated temperatures. The initial grain size cast at 760 °C (464±41 μm) is ~100 μm finer than that cast at 680 and 720 °C. This suggests that the high casting temperature could result in a fine grain size under the same cooling condition. However, the largest grain refining efficiency at 760 °C is only 33.6%, which is much lower than that at 720 °C (50.4%), as shown in Fig. 4(b). Likewise, the grain refining efficiency of limestone is also low (37.3%) at 680 °C. The diverse grain refining efficiency at different temperatures should be deeply related with the dynamic balance between the limestone decomposition and reaction in the magnesium melt.

3.2 Anti-fading capacity of grain refinement

Figure 5 shows the macrographs of suction cast AZ31 alloy with 1.0% limestone at different holding time. The unmodified AZ31 alloy has coarse grains

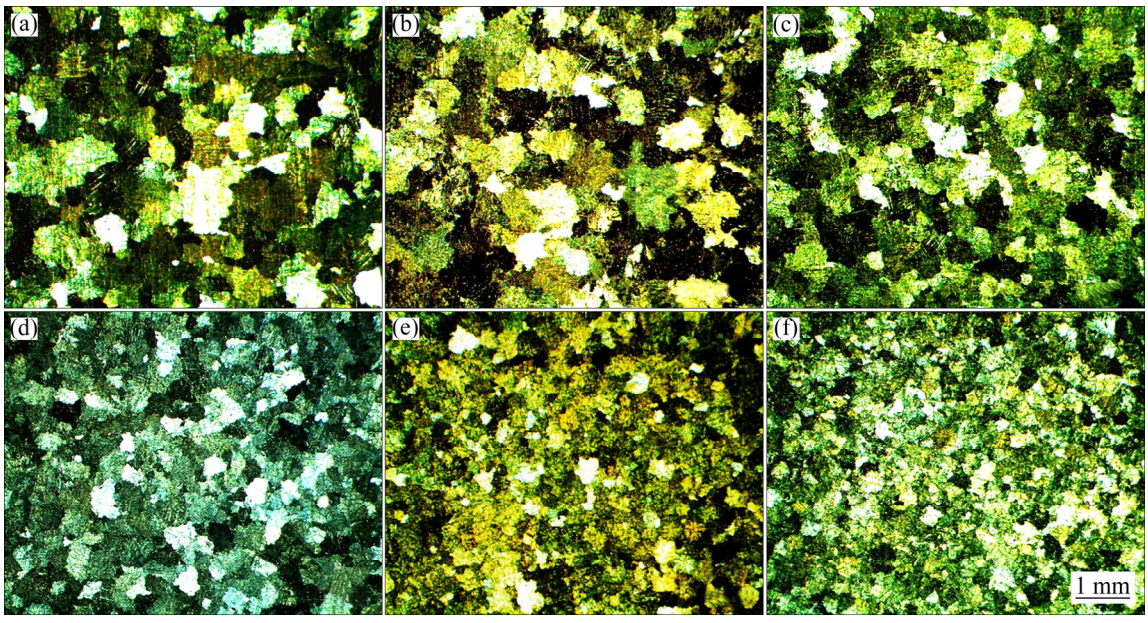

Fig. 2 Grain refining results of limestone additions on gravity casting AZ31 alloys at 720 °C: (a) Unmodified; (b) 0.1%; (c) 0.3%; (d) 0.5%; (e) 1.0%; (f) 2.0%

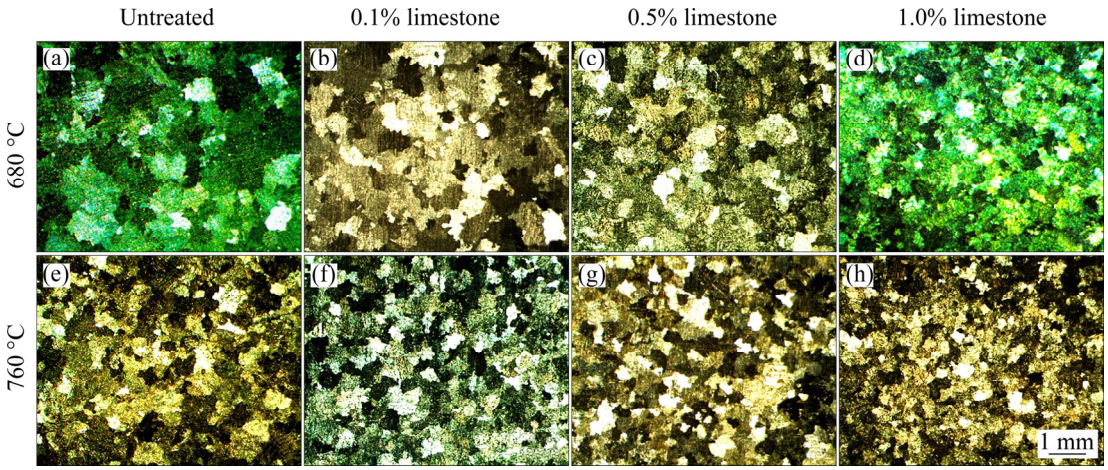

Fig. 3 Grain refining results of limestone addition on gravity casting AZ31 alloys at other inoculating temperatures

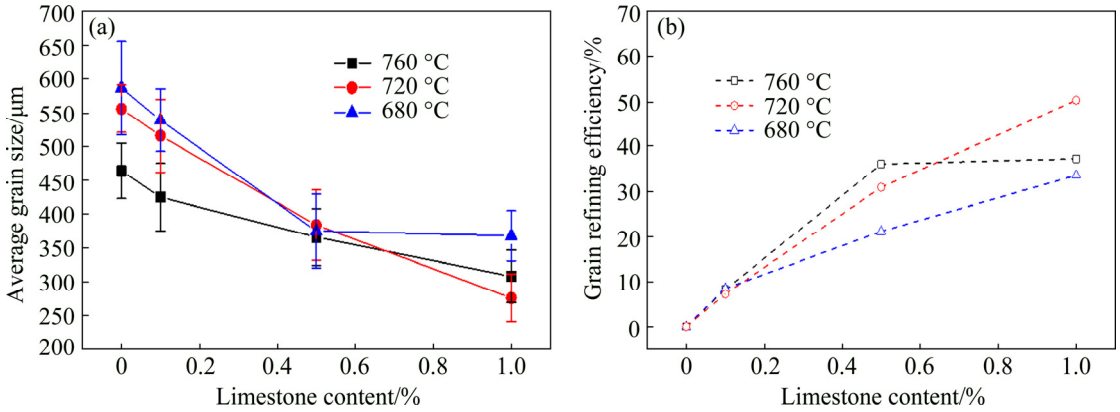

Fig. 4 Grain refining potency of limestone particles on AZ31 alloy vs addition level at different temperatures: (a) Average grain size; (b) Grain refining efficiency

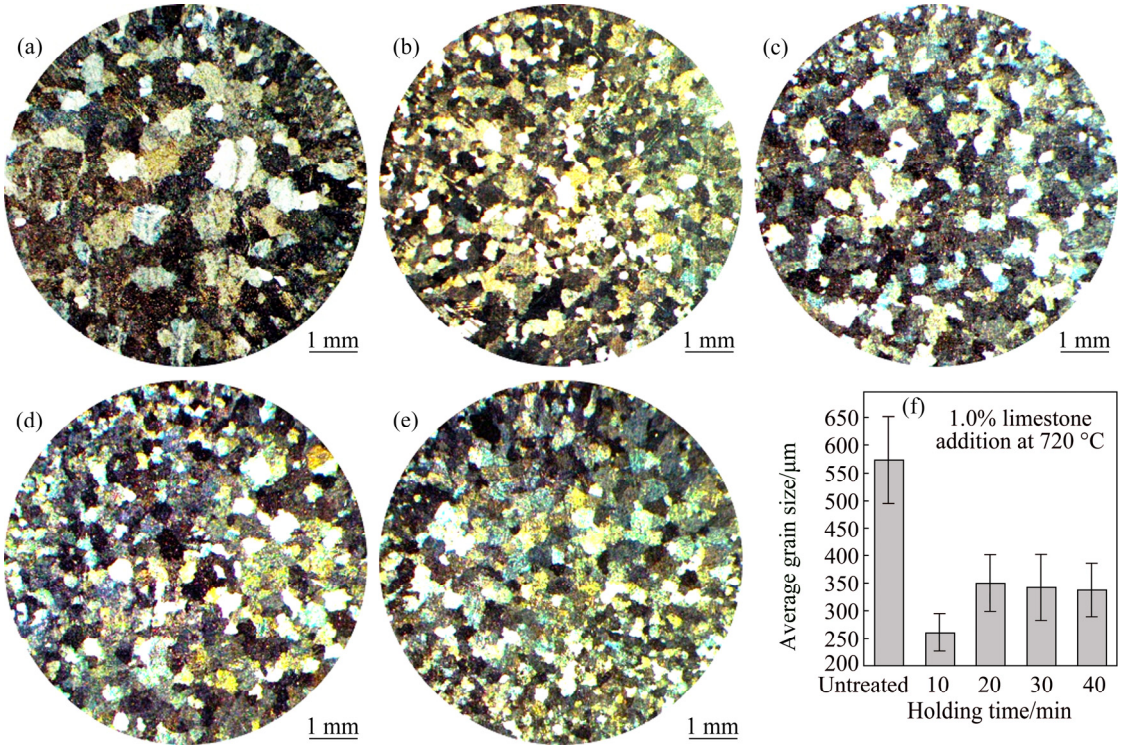

Fig. 5 Effect of holding time on macrostructure of suction cast AZ31 alloy with 1.0% limestone: (a) Unmodified; (b) 10 min; (c) 20 min; (d) 30 min; (e) 40 min; (f) Average grain size vs holding time

((573±79) μm) in the center of casting samples, as shown in Fig. 5(a). The grain size drastically is reduced down to (261±34) μm by 1.0% limestone addition after holding for 10 min, as shown in Fig. 5(b). When the holding time is prolonged to 20 min, the grain size increases slightly, as shown in Fig. 5(c). However, no significant grain growth occurs with further prolonging the holding time. The grain size is around 350 μm, as shown in Fig. 5(e).

3.3 Grain refinement assisted by ultrasound

Figure 6 shows the optical micrographs of gravity casting AZ31 alloys with combinative ultrasonic treatment and limestone addition. The average grain size of AZ31 alloy with ultrasonic treatment is (394±41) μm, indicating that the grain refining efficiency of ultrasonic treatment is still stronger than that of 0.3% limestone. Furthermore, it receives a strong grain refining effect by combining 5 min ultrasonic treatment and 0.3% limestone addition, as shown in Fig. 6(b). The average grain size is (317±23) μm. This suggests that the ultrasound improves the grain refining potency of limestone on AZ31 alloys.

4 Discussion

4.1 Grain refining mechanism of limestone

Because carbon inoculation is only effective for Al-based magnesium alloys, the underlying dispute is the specific kind of aluminum carbide which plays a key role in the grain refinement. EMLEY [13], QIAN and CAO [14] referred that the aluminum carbide (Al_2CO) dominated the grain refining behaviors of carbon inoculation based on the hypothesis of Al_4C_3. HUANG et al [15] considered that Al_2MgC_2 was more potent than Al_4C_3 in terms of the crystallographic matching. DU et al [16] found the potential Al−C−O−Fe rich particles in addition to Al−C−O in the center of Mg grains. The following discussion tries to discuss grain refining mechanism of raw limestone, based on the observations in this work and the proposed view points in literatures.

When the limestone particles were added into the magnesium melt, the thermal decomposition rapidly occurred and carbon dioxide was captured by magnesium melt as follows:

$$CaCO_3(s)\rightarrow CaO(s)+CO_2(g) \quad (2)$$

$$2Mg(l)+CO_2(g)\rightarrow C(s)+2MgO(s) \quad (3)$$

Figure 7 shows the SEM images of as-cast AZ31 alloys with and without limestone addition. The unmodified AZ31 alloy mainly consists of α-Mg, dots-like and needle-like phases, as shown in Figs. 7(a) and (c). Table 2 lists the chemical compositions of these phases by EDX analysis. The chemical composition of the dot-like phase (point *A* in Fig. 7(c)) is Mg−24.9%Al−10.8%Zn (mole fraction), indicating the common $Mg_{17}(Al, Zn)_{12}$ phase in Mg−Al alloys. The needle-like phase (point *B* in Fig. 7(c)) mainly contains Al and Mn elements, suggesting the Al−Mn phase. The modified AZ31 alloy also contains the dot-like $Mg_{17}(Al, Zn)_{12}$ phase and needle-like Al−Mn phase, as shown in Figs. 7(b) and (d). Some carbon-containing particles are additionally observed (point *D* in Fig. 7(d)). These carbon-containing particles should be captured by magnesium melt through Eq. (2). Furthermore, minor Al element is also found in the particles, implying that the alloying Al is capable of bonding carbon in magnesium melt.

Interestingly, some additional Al−Mn−C particles are also observed in the modified AZ31 alloys, as shown by the SEM mapping result in Fig. 8. However, the observed Al−Mn−C particles do not seem to be a single phase in this work, because the Mn and C elements are not totally overlapped in these particles, as shown in Figs. 8(d) and (e). Meanwhile, these Al−Mn−C particles are composed of a two-layer stacking structure (dark and bright contrast), as shown in Fig. 8(f). The two layers with different contrasts correspond to the Al−C (dark contrast) and Al−Mn phase (bright contrast),

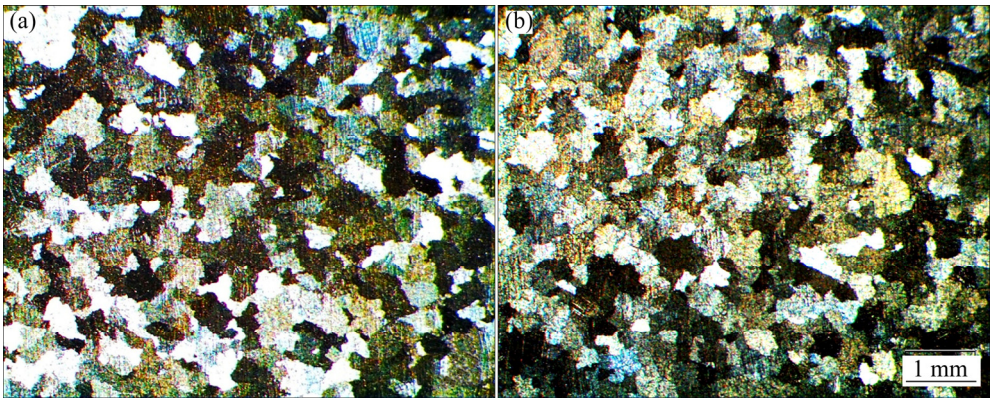

Fig. 6 Combinative grain refining effects of ultrasonic treatment and limestone addition on gravity casting AZ31 alloys at 720 °C: (a) With ultrasound treatment for 5 min; (b) With both 5 min ultrasonic treatment and 0.3% limestone addition

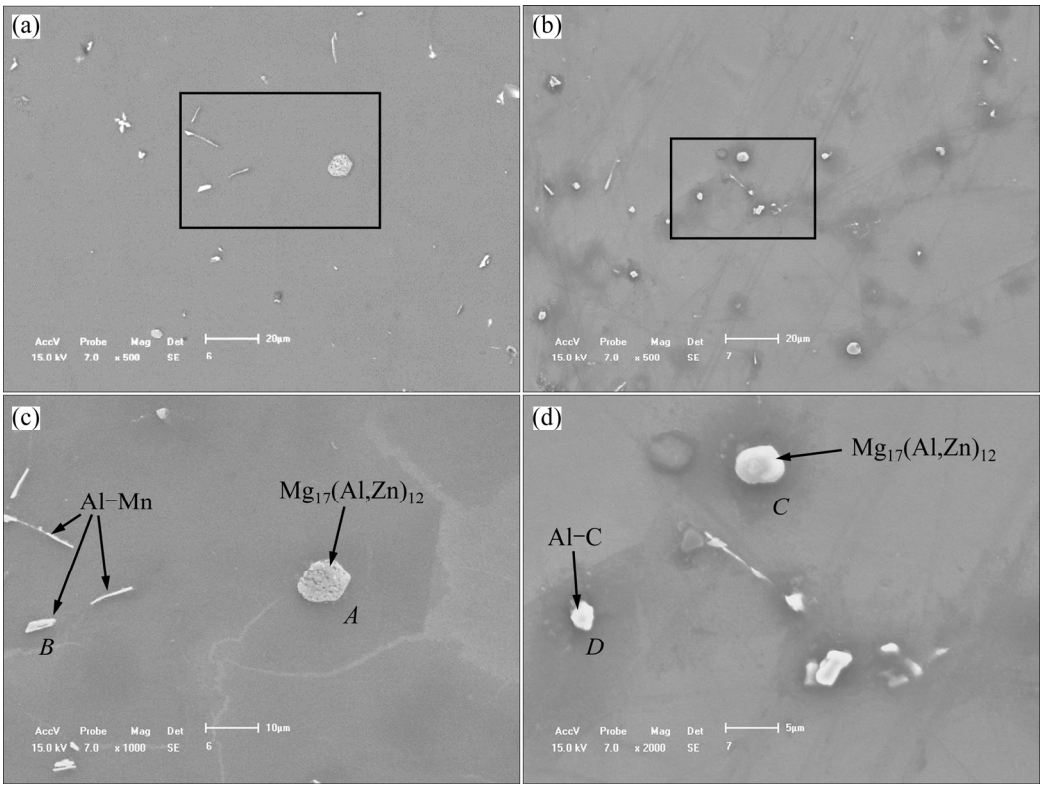

Fig. 7 SEM images of as-cast AZ31 alloys with and without limestone addition: (a, c) Unmodified AZ31 alloy; (b, d) AZ31 alloy with 1% limestone

Table 2 EDS results of untreated AZ31 alloy and AZ31 alloy treated with 1% limestone (mole fraction, %)

Point in Fig. 7	Mg	Al	Zn	Mn	C
A	64.3	24.9	10.8	–	–
B	4.8	46.6	–	48.6	–
C	58.7	30.9	10.4	–	–
D	32.8	3.4	–	–	63.8

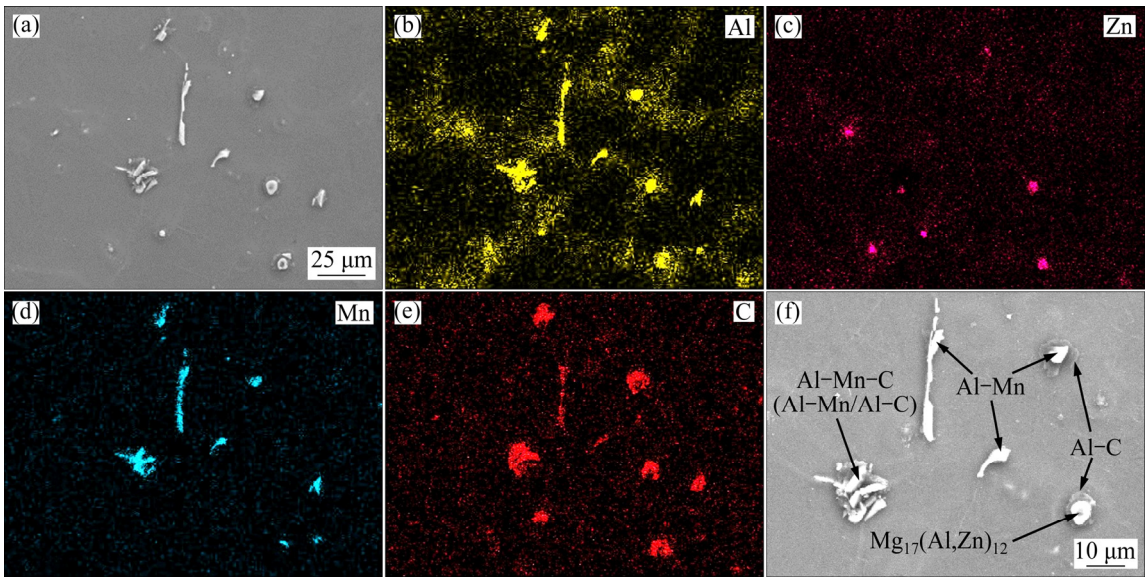

Fig. 8 SEM images of as-cast AZ31 alloys with limestone addition: (a) SEM image; (b) SEM mapping of Al; (c) SEM mapping of Zn; (d) SEM mapping of Mn; (e) SEM mapping of C; (f) Magnifying image of (a)

respectively. Hence, the observed Al−Mn−C particles are actually a kind of duplex Al−C/Al−Mn phase. This possibly demonstrates that the Al−C particles are the potential nuclei for Al−Mn phase.

Figure 9(a) shows that a quantity of particles are observed inside the grains of AZ31 alloy with limestone addition. One of these particles contains grey and bright parts at different orientations, as shown in Fig. 9(b). EPMA was also conducted to examine the chemical composition of this double-layer phase, as shown in Figs. 9(c) and (d). The dark contrast (point *A*) mainly contains 52.7% C, 46.0% Mg, 0.9% Al (mole fraction) and minor amount of Mn, while the chemical composition of the bright part (point *B*) is Mg−29.3%Al−25.8%Mn−18%C−1.3%Fe (mole fraction). Thus, it further confirms that the observed double-layer phase should be the duplex Al−C/Al−Mn−(Fe) phase.

Till now, the role of Al−Mn particles in the grain refining capabilities of carbon inoculations has not been fully understood. Table 3 [3,17−22] lists the reported role of Mn in the grain refinement of Mg−Al based alloys by carbon inoculation. A duplex nucleation hypothesis (Al_4C_3→Al_8Mn_5→α-Mg) has been proposed besides the Al_4C_3 nucleation hypothesis [17,18]. ZHANG et al [3] also declared that the Al−Mn−C or Al−C−Mn particles were responsible for grain refinement of AZ31 by Al−5C addition. However, the Al_8Mn_5 was claimed as a poor nucleus for α-Mg [19], and HAN et al [20] declared the Al_8Mn_5 phase played a restricting role in the nucleation efficiency of Al_4C_3. EASTON et al [21] added a certain amount of Mn to the Mn-free Mg−Al alloys with carbon inoculation, and the

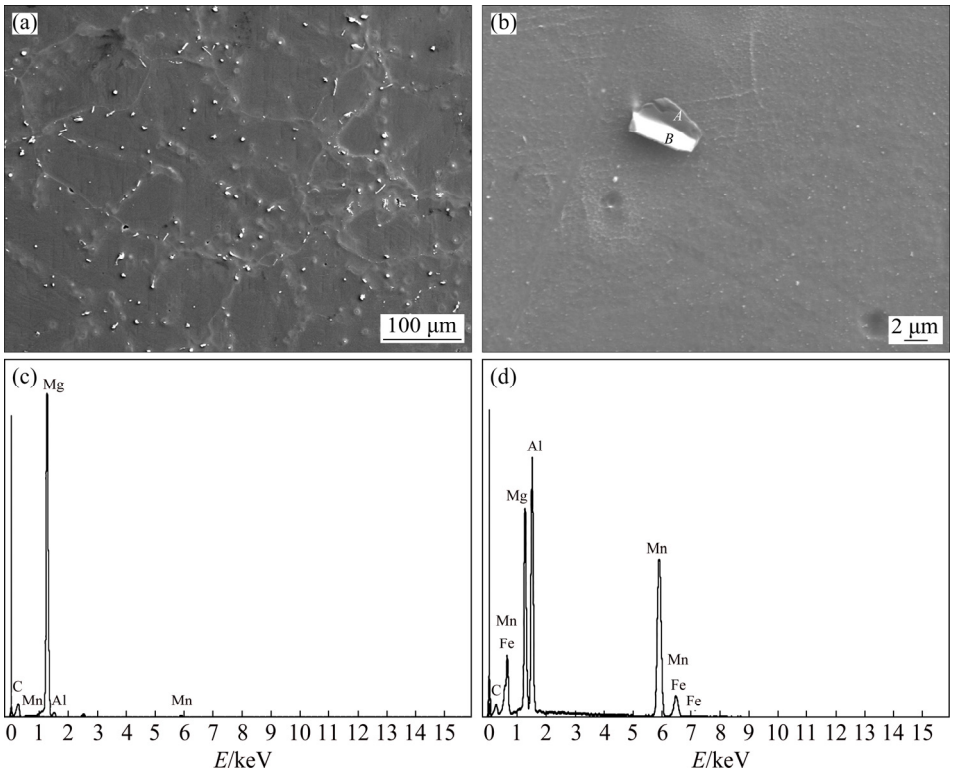

Fig. 9 EPMA results of as-cast AZ31 alloy with limestone addition: (a) SEM image of as-cast AZ31 alloy with limestone addition; (b) Double-layer particle in EPMA; (c, d) EDX spectra of dark part (*A*) and bright parts (*B*) in (b), respectively

Table 3 Role of Mn in grain refinement of Mg−Al based alloys by carbon inoculation [3,17−22]

Alloy	Adding source	Grain refining mechanism
AZ91	C_2Cl_6	Al carbides→$Al_8(Mn,Fe)_5$→α-Mg
Mg−Al (<3% Al)	Al_4C_3	Al_4C_3→α-Mg
Mg−Al containing Mn	Al_4C_3	Al_4C_3→Al_8Mn_5→α-Mg
AZ91D	Mg−50%Al_4C_3, Mn75	Al−C−O−Mn−Fe→α-Mg
AZ31	Al−5%C master alloy	Al−C−Mn as nuclei
Mg−2%Al	SiC, $MnCl_2$ flake	Mn poisoned Al_4C_3
Mg−9%Al	Al−3C master alloy	Clustered Al_4C_3→α-Mg
AZ91	Al−3C master alloy	Clustered Al_4C_3/Al_8Mn_5→α-Mg

added Mn might be poisonous to the inoculated nuclei in the melt. Nevertheless, this disputable role of Mn may be due to different adding sources of Mn and processing method, and the pre-existed Mn in the melt might have different influences on the carbon inoculations.

In this work, the similar Al−C/Al−Mn particles are also observed, suggesting that the duplex nucleation may be still plausible. However, the Al−C layer in the double-layer particles contains only about 0.9% Al (mole fraction) element, which is much different from the case of Al−C compound additions [17,18]. It is reasonable due to different carbon sources. As discussed above, the magnesium melt captures carbon as a form of CO_2 gas. Thus, there is additional reaction kinetics to form Al−C phase (Al bonds C). During the undergoing Al−C bond, it is quite possible that the Al−Mn−(Fe) phase could immediately nucleate on these undergoing particles (rich in carbon but poor in Al). In other words, there is no need for sufficient bond of Al and C to serve as nuclei for Al−Mn−(Fe) phase. Similarly, the Al content in the single Al−C particles is also very low (3.4% (mole fraction), point *D* in Fig. 7(d)).

Thus, the current work clarifies that the Al−C and Al−C/Al−Mn−(Fe) particles are inoculated to refine AZ31 alloys in different manners. As Al_8Mn_5 phase is practically and theoretically proved to be non-effective nuclei for α-Mg crystals, the observed Al−Mn species may be the potential ε-AlMn or τ-AlMn phase [23,24]. In addition, Fig. 8(f) also shows that some $Mg_{17}(Al, Zn)_{12}$ phases also pile above the Al−C particles. It possibly suggests that the observed Al−C particles are also able to serve as nuclei for $Mg_{17}(Al, Zn)_{12}$ phase.

Figure 10 shows the schematic plot for the grain refining mechanism of limestone on AZ31 alloys. Adding limestone into the melt results in a series of phase evolution. There are a chain of reactions in the melt, including carbonate decomposition and carbon capture, as shown in Figs. 10(a) and (b), respectively. Some Al−C compounds with low Al content can form directly after the carbon capture. It has been reported that

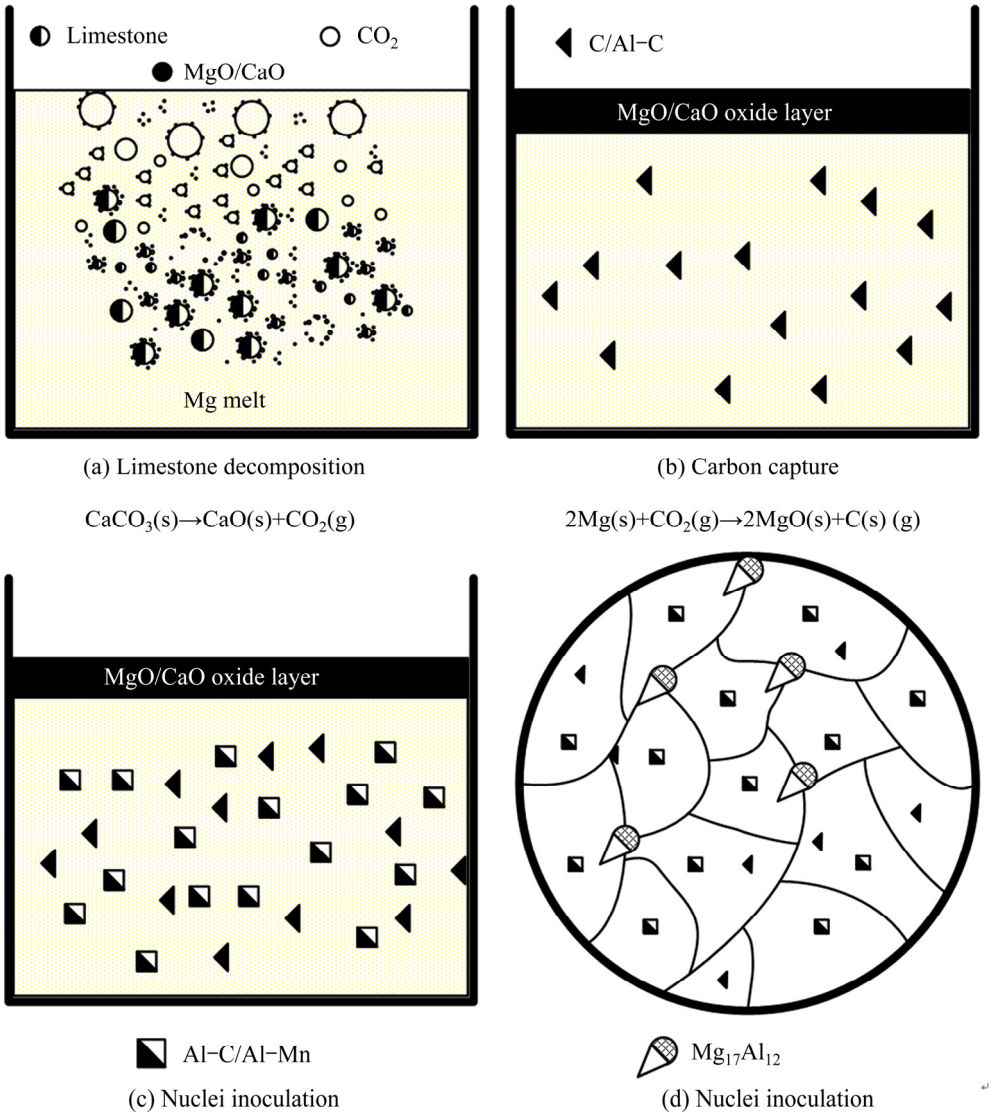

Fig. 10 Schematic plot showing grain refining mechanism of limestone on AZ31 alloys

the AlMn phase precipitates prior to α-Mg [11]. Then, a number of heterogeneous Al−C/Al−Mn−(Fe) can be inoculated on the early precipitated Al−C particles, as shown in Fig. 10(c). Thus, it can be predicted that the phase evolution in the melt involves a formation of duplex Al−C−Mn phase nucleated on the early inoculated Al−C particles. Finally, the microstructure is much refined with Al−C or Al−C/Al−Mn in the center of grains (Fig. 10(d)). It should be noted that some $Mg_{17}(Al, Zn)_{12}$ phases are also nucleated on the Al−C particles, as shown in Fig. 8(f).

4.2 Comparison between carbonate and limestone

Figure 11 shows the comparative grain refining results of calcium carbonate addition on gravity casting AZ31 alloys. The calcium carbonate has a poor grain refining potency, compared to limestone particles. The AZ31 alloy with 0.1% calcium carbonate addition even has a coarser grain size ((650±67) μm) than the unmodified alloy, as shown in Fig. 11(a). Meanwhile, the grain size reduces slightly as the addition even increases up to 1.0%. The limestone has a much stronger grain refining potency over calcium carbonate. For instance, the grain size with 1.0% limestone addition is only (276±28) μm, much smaller than that with 1.0% calcium carbonate addition ((468±68) μm).

The added calcium carbonate particles belong to the "precipitated" calcium carbonate, which are manufactured from the solution of calcined heavy raw limestone (lime milk). Thus, the pure calcium carbonate has larger sedimentation ratio than the limestone. By this token, the calcium carbonate loses much more easily than the raw limestone particles during adding process. On the other hand, the smashed limestone consists of some large size particles (>10 μm, Fig. 1(c)). These large size particles can help the smaller size particles go deep into the melt and fully contact with the melt. In addition, the impurity Al_2O_3 in limestone is also beneficial to the grain refinement, because it provides minor amount of necessary solute Al in local areas, through the following reaction:

$$Al_2O_3(s)+3Mg(l)\rightarrow 2Al(l)+3MgO(s) \quad (4)$$

This could increase the number of Al−C particles, which is key to the grain refining potency of limestone particles as discussed above. In a word, the raw limestone has a stronger grain refining potency than the pure calcium carbonate, encouraging the application of low-cost and abundant raw limestone.

4.3 Effects of byproduct CaO

CaO is another reaction product of limestone decomposition. However, its effects on grain refining result have not been discussed yet. The behaviors of CaO in magnesium melt have been widely investigated, and some Ca-containing particles in magnesium alloys have also be found and characterized, such as Mg_2Ca, CaMgSi, and Laves C15 phase [25−27]. The CaO addition can increase the ignition of magnesium alloy [28], due to a more compact and thicker initial oxide layer [25].

However, no Ca-containing phase has been observed in this work. Figure 12 shows the XRD pattern of the oxide layer on the melt surface before casting. The oxide layer mainly consists of MgO, CaO, the remanent

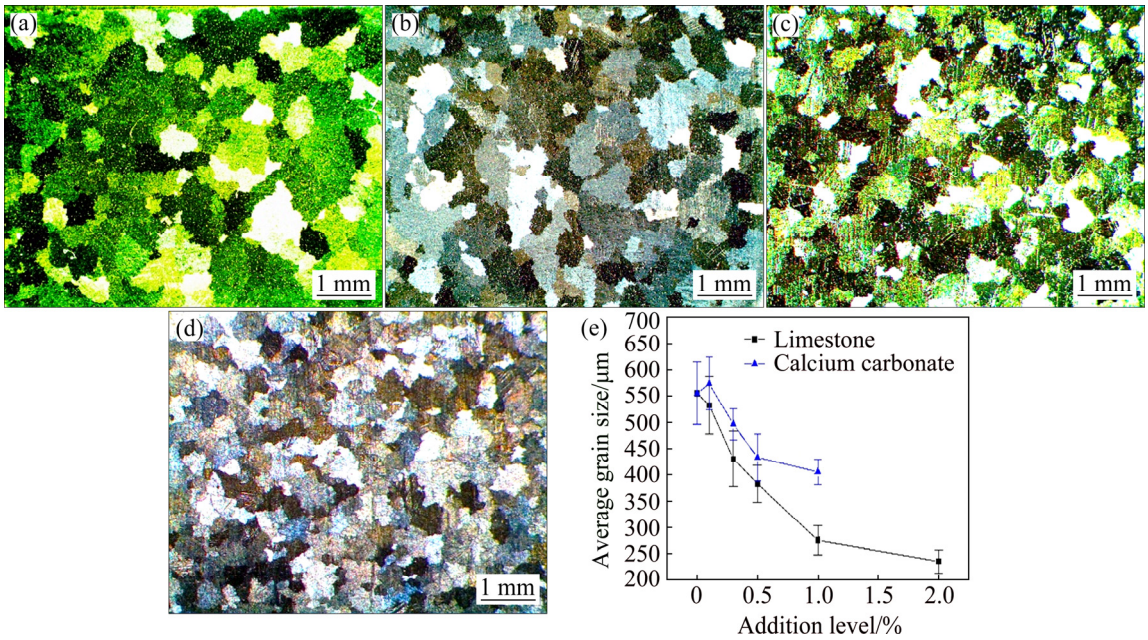

Fig. 11 Grain refining results of calcium carbonate addition on gravity casting AZ31 alloys: (a) 0.1%; (b) 0.3%; (c) 0.5%; (d) 1.0%; (e) Average grain size vs addition level of limestone or calcium carbonate

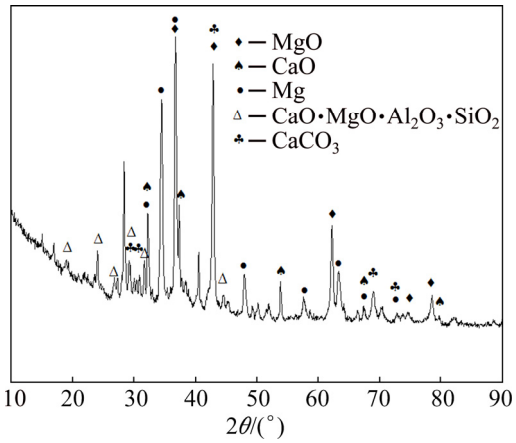

Fig. 12 XRD pattern of oxide layer on melt surface

$CaCO_3$ and some other duplex oxides. CaO is in-situ produced by the thermal decomposition of limestone. As a result, the produced CaO particles have very fine size and high surface activity, compared to the directly added CaO particles. Furthermore, the outgoing CO_2 gas drastically drives these fine CaO particles to the melt surface. They are soon captured by MgO on the melt surface, due to high surface activity. In other words, they have limited influence on the grain refinement by limestone particles.

4.4 Grain refinement enhanced by ultrasound

The combination of ultrasound and limestone addition has a better grain refining potency than the single limestone addition. As the ultrasonic treatment is conducted at about 100 °C above the liquidus, the cavitation-induced nucleation mechanism comes to work [29]. The cavitation may enhance the nucleation events probably through enhancing the wettability of particles. On the other hand, LIU et al [30] reported that the grain refinement by ultrasound faded away with the prolonged holding time. 10 min might be too long to maintain the cavitation-activated particles serving as nuclei in the unmodified alloy.

4.5 Perspective on limestone addition for industry

In this work, the limestone particles have a strong grain refining potency on AZ31 alloys, due to the inoculation of effective nuclei. The underlying mechanism is controlled by the reaction rate of both dissociative limestone (Eq. (2)) and carbon trapping (Eq. (3)). High addition level and temperature are obviously beneficial for the reaction rate. However, the capture capability of ~1 kg magnesium melt has a limitation. Too much fast reaction rate leads to the spare CO_2 gas to go out in vain with severe bubbling and melt loss. Thus, good grain refining efficiency is obtained at proper limestone addition (1.0%, mass fraction) and temperature (720 °C).

On the other hand, the melt could be continuously degassed during the CO_2 gas bubble rising through the melt. The hydrogen content reduces from 15 to 10 μg/g after limestone addition at 720 °C. It could inhibit the microporosity and promote the mechanical properties [12]. Thus, the limestone addition can achieve reliable grain refinement and degassing at the same time. It is considerable for the extensive application of limestone to refine Mg−Al based alloys in magnesium industry, due to its low cost, high purity (no need for mineral separation) and broad source.

5 Conclusions

1) The limestone particles have a good grain refining potency on the AZ31 alloys. The grain size reduces by half from (556±60) to (236±22) μm at the limestone addition and temperature of 2.0% and 720 °C, respectively. The limestone addition over 1.0% becomes less effective.

2) The grain refinement by limestone has a good anti-fading capacity without any significant grain coarsening in a holding time as long as 40 min.

3) The inoculated Al−C and Al−C/Al−Mn−(Fe) particles are considered as potent nuclei for Mg grains. The grain refining potency of limestone could be enhanced by ultrasound through cavitation-enhanced nucleation mechanism.

4) The limestone has a stronger grain refining potency over the pure calcium carbonate, not only because of the unique particle size distribution and compact structure, but also due to the beneficial impurity Al_2O_3, providing necessary solute Al.

References

[1] HAN Guang, LIU Xiang-fa, DING Hai-min. Grain refinement of AZ31 magnesium alloy by new Al−Ti−C master alloys [J]. Transactions of Nonferrous Metals Society of China, 2009, 19: 1057−1064.

[2] YANG Ming-bo, PAN Fu-sheng, CHENG Ren-ju, TANG Ai-tao. Effects of Al−10Sr master alloys on grain refinement of AZ31 magnesium alloy [J]. Transactions of Nonferrous Metals Society of China, 2008, 18: 52−58.

[3] ZHANG Ai-min, HAO Hai, ZHANG Xing-guo. Grain refinement mechanism of Al−5C master alloy in AZ31 magnesium alloy [J]. Transactions of Nonferrous Metals Society of China, 2013, 23: 3167−3172.

[4] JIANG Zhong-tao, JIANG Bin, ZHANG Jian-yue, DAI Jia-hong, YANG Qing-shan, YANG Qin, PAN Fu-sheng. Effect of Al_2Ca intermetallic compound addition on grain refinement of AZ31 magnesium alloy [J]. Transactions of Nonferrous Metals Society of China, 2016, 26: 1284−1293.

[5] DU Jun, WANG Hai-lei, ZHOU Ming-chuan, LI Wen-fang. Poisoning-free effect of calcium on grain refinement of Mg−3%Al alloy containing trace Fe by carbon inoculation [J]. Transactions of

Nonferrous Metals Society of China, 2013, 23: 307−314.
[6] ZHANG M X, KELLY P M, QIAN M, TAYLOR J A. Crystallography of grain refinement in Mg−Al based alloys [J]. Acta Materialia, 2005, 53: 3261−3270.
[7] JIN Q L, EOM J P, LIM S G, PARK W W, YOU B S. Effects of C_2Cl_6 addition on grain refinement and mechanical properties of AZ31 magnesium alloy [J]. Metals and Materials International, 2003, 9: 453−458.
[8] LU L, DAHLE A K, STJOHN D H. Grain refinement efficiency and mechanism of aluminium carbide in Mg−Al alloys [J]. Scripta Materialia, 2005, 53: 517−522.
[9] GAO Sheng-yuan, CUI Jian-zhong, LE Qi-chi, ZHANG Zhi-qiang. The research on the effect of $MgCO_3$ on the grain refinement in AZ31 magnesium alloy [J]. Materials Science and Engineering Technology, 2010, 41: 652−656.
[10] YANO E, TAMURA Y, MOTEGI T, SATO E. Effect of pure carbon powder on grain refining of cast magnesium alloy AZ91 [J]. Journal of Japan Institute of Light Metals, 2001, 51: 599−603.
[11] KIM Y M, WANG L, YOU B S. Grain refinement of Mg−Al cast alloy by the addition of manganese carbonate [J]. Journal of Alloys and Compounds, 2010, 490: 695−699.
[12] LIU Xuan, ZHANG Zhi-qiang, HU Wen-yi, LE Qi-chi, BAO Lei, CUI Jian-zhong, JIANG Jia-jia. Study on hydrogen removal of AZ91 alloys using ultrasonic argon degassing process [J]. Ultrasonics Sonochemistry, 2015, 26: 73−80.
[13] EMLEY E F. Principles of magnesium technology [M]. London: Pergamon Press, 1966.
[14] QIAN M, CAO P. Discussions on grain refinement of magnesium alloys by carbon inoculation [J]. Scripta Materialia, 2005, 52: 415−419.
[15] HUANG Yuan-ding, KAINER K U, HORT N. Mechanism of grain refinement of Mg−Al alloys by SiC inoculation [J]. Scripta Materialia, 2011, 64: 793−796.
[16] DU Jun, YANG Jian, KUWABARA M, LI Wen-fang, PENG Ji-hua. Effect of iron and/or carbon on the grain refinement of Mg−3Al alloy [J]. Materials Transactions, 2007, 48: 2903−2908.
[17] NIMITYONGSKUL S, JONES M, CHOI H, LAKES R, KOU S, LI X. Grain refining mechanisms in Mg−Al alloys with Al_4C_3 microparticles [J]. Materials Science and Engineering A, 2010, 527: 2104−2111.
[18] KIM Y M, YIM C D, YOU B S. Grain refining mechanism in Mg−Al base alloys with carbon addition [J]. Scripta Materialia, 2007, 57: 691−694.
[19] WANG Y, XIA M, FAN Z, ZHOU X, THOMPSON G E. The effect of Al_8Mn_5 intermetallic particles on grain size of as-cast Mg−Al−Zn AZ91D alloy [J]. Intermetallics, 2010, 18: 1683−1689.
[20] HAN Meng-xia, ZHU Xiang-zhen, GAO Tong, LIU Xiang-fa. Revealing the roles of Al_4C_3 and Al_8Mn_5 during α-Mg nucleation in Mg−Al based alloys [J]. Journal of Alloys and Compounds, 2017, 705: 14−21.
[21] EASTON M A, SCHIFFL A, YAO J Y, KAUFMANN H. Grain refinement of Mg−Al(−Mn) alloys by SiC additions [J]. Scripta Materialia, 2006, 55: 379−382.
[22] LIU Sheng-fa, ZHANG Yuan, HAN Hui. Role of manganese on the grain refining efficiency of AZ91D magnesium alloy refined by Al_4C_3 [J]. Journal of Alloys and Compounds, 2010, 491: 325−329.
[23] CAO P, QIAN M, STJOHN D H Effect of manganese on grain refinement of Mg−Al based alloys [J]. Scripta Materialia, 2006, 54: 1853−1858.
[24] QIU D, ZHANG M X, TAYLOR J A, FU H M, KELLY P M. A novel approach to the mechanism for the grain refining effect of melt superheating of Mg−Al alloys [J]. Acta Materialia, 2007, 55: 1863−1871.
[25] LEE T W, KIM H G, SO M G, LEE J K, KIM S K, PARK W J, KIM W Y, KIM S, LIM S H. Microstructural evaluation of oxide layers in CaO-added Mg alloys [J]. Journal of Alloys and Compounds, 2015, 635: 5−10.
[26] JEONG J, IM J, SONG K, KWON M, KIM S K, KANG Y B, OH S H. Transmission electron microscopy and thermodynamic studies of CaO-added AZ31 Mg alloys [J]. Acta Materialia, 2013, 61: 3267−3277.
[27] KONDOH K, FUJITA J, UMEDA J, IMAI H, ENAMI K, OHARA M, IGARASHI T. Thermo-dynamic analysis on solid-state reduction of CaO particles dispersed in Mg−Al alloy[J]. Materials Chemistry and Physics, 2011, 129: 631−640.
[28] LEE J K, KIM S K. Effect of CaO composition on oxidation and burning behaviors of AM50 Mg alloy [J]. Transactions of Nonferrous Metals Society of China, 2011, 21(S1): s23−s27.
[29] WANG Feng, ESKIN D, CONNOLLEY T, MI Jia-wei. Influence of ultrasonic treatment on formation of primary Al3Zr in Al−0.4Zr alloy [J]. Transactions of Nonferrous Metals Society of China, 2017, 27: 977−985.
[30] LIU Xuan, ZHANG Jian-feng, LI Hao-yu, LE Qi-chi, ZHANG Zhi-qiang, HU Wen-yi, BAO Lei. Electrical resistivity behaviors of liquid Pb−Sn binary alloy in the presence of ultrasonic field [J]. Ultrasonics, 2015, 55: 6−9.

石灰石矿石对铸态 AZ31 镁合金晶粒细化效果的影响

刘 轩[1]，尹思奇[2]，张志强[2]，乐启炽[2]，薛济来[1]

1. 北京科技大学 冶金与生态工程学院，北京 100083；
2. 东北大学 材料电磁过程教育部重点实验室，沈阳 110819

摘 要：采用晶粒细化试验和显微组织观察研究石灰石矿石对铸态 AZ31 镁合金的晶粒细化效果。结果表明：石灰石矿石可显著细化 AZ31 镁合金晶粒，且细化效果与石灰石添加量和熔化温度密切相关。最佳石灰石添加量和熔化温度分别为 2.0%(质量分数)和 720 °C，AZ31 合金的平均晶粒尺寸由(556±60) μm 减小至(236±22) μm，抗衰退时间长达 40 min。石灰石细化机制与反应孕育 Al−C 及 Al−C/Al−Mn−(Fe)为 α-Mg 有效形核核心有关。超声空化诱导形核可进一步强化石灰石矿石的细化效果。

关键词：AZ31 镁合金；晶粒细化；石灰石矿石；显微组织；超声处理

(Edited by Wei-ping CHEN)